Engineered Mononuclear Variants in *Bacillus cereus* Metallo-β-lactamase BcII Are Inactive[†]

Luciano A. Abriata,[‡,§] Lisandro J. González,[‡,§] Leticia I. Llarrull,[‡] Pablo E. Tomatis,[‡] William K. Myers,[||] Alison L. Costello,[||] David L. Tierney,[||] and Alejandro J. Vila*[,‡]

IBR (Instituto de Biología Molecular y Celular de Rosario), CONICET, Facultad de Ciencias Bioquímicas y Farmacéuticas, Universidad Nacional de Rosario, Suipacha 531, (S2002LRK) Rosario, Argentina, and Department of Chemistry and Chemical Biology, University of New Mexico, Albuquerque, New Mexico 87131

Received April 18, 2008; Revised Manuscript Received June 13, 2008

ABSTRACT: Metallo-β-lactamases (MβLs) are zinc enzymes able to hydrolyze almost all β-lactam antibiotics, rendering them inactive, at the same time endowing bacteria high levels of resistance. The design of inhibitors active against all classes of MβLs has been hampered by their structural diversity and by the heterogeneity in metal content in enzymes from different sources. BcII is the metallo-β-lactamase from *Bacillus cereus*, which is found in both the mononuclear and dinuclear forms. Despite extensive studies, there is still controversy about the nature of the active BcII species. Here we have designed two mutant enzymes in which each one of the metal binding sites was selectively removed. Both mutants were almost inactive, despite preserving most of the structural features of each metal site. These results reveal that neither site isolated in the MβL scaffold is sufficient to render a fully active enzyme. This suggests that only the dinuclear species is active or that the mononuclear variants can be active only if aided by other residues that would be metal ligands in the dinuclear species.

β-Lactam antibiotics are potent antibacterial agents, since they irreversibly inhibit the transpeptidases involved in the process of cell wall cross-linking in bacteria, leading to bacteriolysis (*1*). Bacteria have evolved a variety of strategies to resist the action of β-lactam antibiotics, such as mutations in the target proteins, antibiotic efflux, and antibiotic hydrolysis (*1, 2*). The latter mechanism depends on the expression of enzymes called β-lactamases that hydrolyze the β-lactam ring characteristic of this class of antibiotics (*1–3*). Hydrolyzed β-lactams are no longer capable of binding to their target proteins and are hence rendered ineffective.

The lactamases can be divided into serine-lactamases (SβLs,[1] classes A, C, and D) and metallo-β-lactamases (MβLs, class B) (*1, 4*). SβLs present a serine residue in the active site that is the nucleophile that attacks the β-lactam ring, giving rise to a covalently bound intermediate with the β-lactam amide bond hydrolyzed. MβLs make up one of the latest generation of clinically relevant β-lactamases. These enzymes contain one or two Zn(II) ions in the active sites, and activity is metal-dependent (*4, 5*). These enzymes are capable of hydrolyzing all known classes of β-lactam antibiotics, and some of them are plasmid encoded and hence can spread easily among bacteria. The clinically used lactamase inhibitors, such as clavulanic acid, are active against only SβLs (*6*) but not against MβLs, which present a different catalytic mechanism (*7*).

MβLs display a low degree of sequence homology but share the same fold. MβLs are classified into three subclasses, B1, B2, and B3, based on amino acid sequence homology (*8, 9*). The first crystal structure determined for an MβL was that of the subclass B1 enzyme BcII from *Bacillus cereus* and revealed one Zn(II) ion bound to three His residues (His116, His118, and His196) and a H_2O/OH^- molecule, in the so-called Zn1 or 3H site (Figure 1A) (*10*). Spectroscopic studies (*11*) and subsequent structures of BcII and other B1 MβLs revealed a dinuclear metal center containing the tetrahedral 3H site and an additional trigonal bipyramidal Zn(II) site (the Zn2 or DCH site), where the metal ion is coordinated to Asp120, Cys221, His263, a bridging H_2O/OH^- molecule, and an additional water molecule (Figure 1B) (*12*). Most B3 enzymes are dinuclear metalloproteins and contain the 3H site and a site analogous to the DCH site in B1 MβL, which is defined by Asp120, His121, and His263 (and is

[†] This work was supported by grants from ANPCyT and HHMI to A.J.V. and from the National Institutes of Health (NIH NCRR P20RR-16480) to D.L.T. The 600 MHz NMR spectrometer was purchased with funds from ANPCyT (PME2003-0026) and CONICET. L.A.A. and L.J.G. are recipients of doctoral fellowships from CONICET and ANPCyT, respectively, L.I.L. was the recipient of a doctoral fellowship from CONICET, and P.E.T. was the recipient of a postdoctoral fellowship from CONICET. A.J.V. is a staff member from CONICET and an International Research Scholar of the Howard Hughes Medical Institute.

* To whom correspondence should be addressed. Phone: +54-341-4350661, ext. 108. Fax: +54-341-4390465. E-mail: vila@ibr.gov.ar.

[‡] Universidad Nacional de Rosario.

[§] These authors contributed equally to this paper.

[||] University of New Mexico.

[1] Abbreviations: BcII, β-lactamase II from *Bacillus cereus*; CD, circular dichroism; DTNB, 5,5′-dithiobis(2-nitrobenzoate); EDTA, ethylenediaminetetraacetic acid; EXAFS, extended X-ray absorption fine structure; GST, glutathione *S*-transferase; HEPES, *N*-(2-hydroxyethyl)piperazine-*N*′-2-ethanesulfonic acid; MβL, metallo-β-lactamase; LMCT, ligand-to-metal charge transfer; NMR, nuclear magnetic resonance; PAR, 4-(2-pyridylazo)resorcinol; PMSF, phenylmethanesulfonyl fluoride; SβL, serine-β-lactamase; SDS−PAGE, sodium dodecyl sulfate−polyacrylamide gel electrophoresis; WT, wild type.

10.1021/bi8006912 CCC: $40.75
Published on Web 07/25/2008

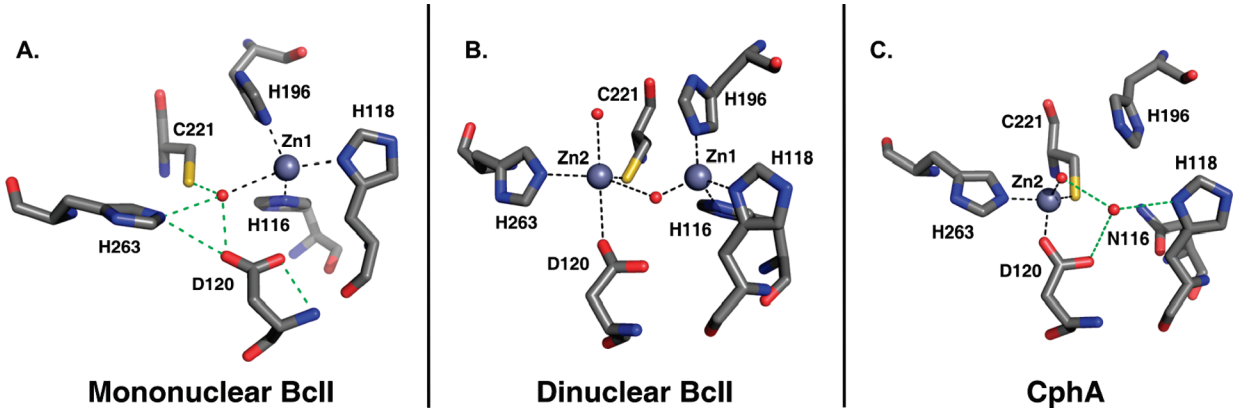

FIGURE 1: Active site structures of BcII (B1 subclass) and CphA (B2 subclass). (A) Mononuclear form of BcII as revealed by crystallography (PDB entry 1bmc), showing the H-bond network determined by Dal Peraro et al. (*10, 48*). (B) Structure of the dinuclear form of BcII as revealed by crystallography (PDB entry 1bc2) (*12*). (C) CphA active site in the resting enzyme, as calculated by Simona et al. (*17, 49*). Metal ligand coordination bonds are shown as black dashed lines while H-bonds as green dashed lines. Water molecules are depicted as red spheres.

therefore named the DHH site) (*13, 14*). A mononuclear B3 enzyme, GOB, was recently reported to be fully active with only one metal ion bound at the DHH site (*15*). Class B2 enzymes are only active as mononuclear enzymes, with the only Zn(II) ion located in the DCH site (Figure 1C) (*16–18*). This diversity in terms of the number and location of the bound metal ions and in terms of the metal ligands has so far thwarted most attempts to assess the specific activity of each species and, as a consequence, the elucidation of a common mechanism of hydrolysis among all MβL subclasses (*4*).

Mononuclear and dinuclear BcII coexist over a wide range of metal ion concentrations (*19–21*). Hence, it is impossible to have mononuclear WT BcII isolated to study its kinetic and spectroscopic properties. Several point mutants were designed, where the metal ligands were substituted one by one by residues with weak metal binding capabilities, to obtain protein variants with the metal bound in one site or the other (*22, 23*). However, most of these point mutants exhibited the same complexity as WT BcII, with mixtures of mono- and dinuclear forms at all levels of Zn(II) loading (*20*).

In an attempt to identify and characterize the active mononuclear BcII species, we constructed two mutant proteins: 3H-BcII and DCH-BcII, with the metal bound to the 3H and DCH site, respectively. Here we present a spectroscopic and kinetic characterization of these mononuclear enzymes and show that neither site isolated in the MβL scaffold is sufficient to render a fully active B1 MβL.

EXPERIMENTAL PROCEDURES

Reagents. All chemicals were reagent grade. *Escherichia coli* BL21(DE3)pLysS′ cells (Stratagene, CA) were employed for protein expression. *E. coli* JM109 cells (Stratagene) were employed for transformation with plasmid DNA and ligation mixtures. The Luria-Bertani medium (Sigma) was used as the growth medium for all bacterial strains.

DNA Techniques. DNA preparation and related techniques were performed according to standard protocols (*24*). Plasmid DNA was isolated using the Wizard Plus SV Minipreps kit (Promega). DNA was extracted from agarose gels using either the QIAEX II kit (Qiagen) or GFX columns (Amersham Pharmacia).

Site-Directed Mutagenesis. Site-directed mutagenesis of the wild-type BcII gene was performed using the megaprimer PCR method, as previously described (*25*). The DCH mutant (BcII-H116S/H118S/H196S) was constructed by mutagenizing the NH_2- and CO_2H-terminal coding halves of the wild-type gene separately, contained in plasmids KS-NH_3 and KS-CT_2, respectively (*25*), and then combining them into a cloning vector. In this way, plasmid KS-NH3 was used as a template to introduce the H116S and H118S substitutions simultaneously, employing the *ks-reverse* (5′-CACACAggAAACAgCTATgAC-3′) and mutagenic H116S/H118S_*Pvu*II (5′-CATTATTACATCTgCgTCAgCTgATCgAATTg-3′) primers in the first PCR round and the megaprimer and *ks-forward* primer (5′-TCACACAggAAACAgCTATgAC-3′) in the second PCR. Plasmid KS-CT2, on the other hand, was employed as a template for introduction of the H196S substitution. In this case, the *ks-forward* and H196S_*Sal*I (5′-ATTATCTTCTgTCgACCCTTTCCCTgg-3′) primers were used in the first PCR while the resulting megaprimer and primer *ks-reverse* were employed in the second one. Mutagenic primers were designed to introduce a recognition site for the restriction endonucleases *Pvu*II (H116S/H118S_*Pvu*II) and *Sal*I (H196S_*Sal*I primer), through the introduction of a silent mutation proximal to the mutation of interest (primer tailoring). The mutant halves were then reamplified, digested with endonucleases *Bam*HI and *Pst*I, for the NH_2-terminal coding fragment, and *Pst*I and *Hin*dIII for the corresponding CO_2H-terminal half, and then simultaneously ligated into a pBluescript II SK(−) cloning vector previously digested with endonucleases *Bam*HI and *Hin*dIII.

The 3H mutant gene (BcII-D120S/C221S) was constructed as follows. Plasmid pBSNtD120S containing the gene sequence encoding the BcII-D120S mutant was digested with *Bam*HI and *Pst*I endonucleases, while plasmid pBSCtC221S, containing the gene encoding the BcII-C221S mutant, was digested with *Pst*I and *Hin*dIII endonucleases. The released fragments were purified and simultaneously ligated to a pBluescript II SK(−) cloning vector previously digested with endonucleases *Bam*HI and *Hin*dIII.

Ligation mixtures were transformed into *E. coli* JM109. Plasmid preparations from colonies carrying constructs of the correct size were digested with *Pvu*II and *Sal*I endonu-

cleases (DCH), and *Sph*I and *Sal*I endonucleases (3H), to verify the presence of the desired mutations. The entire mutant sequences were ultimately confirmed by DNA sequencing (University of Maine Sequencing Facility).

Finally, the 3H and DCH mutant genes were independently subcloned into the pET-TERM expression plasmids through the *Bam*HI and *Hin*dIII restriction sites (*26*). This expression vector allows the overproduction of the protein of interest as an N-terminal fusion to GST from *Schistosoma japonicum*, under the control of the T7 promoter. In addition, pET-TERM contains the BcII gene termination sequence from *B. cereus*.

Enzyme Purification. The DCH and 3H mutants were expressed in *E. coli* BL21(DE3)pLysS′ cells as GST fusion proteins, purified, digested with thrombin, and finally separated from GST as described previously (*25*). The yields were typically 15−20 mg of DCH/L of culture and 20−30 mg of 3H/L of culture. The correct folding of the mutants was verified by circular dichroism spectra of 30 μM protein samples in 10 mM Tris-HCl and 50 mM NaCl (pH 7.5) at 25 °C, using a Jasco J-715 spectropolarimeter flushed with N_2 (data not shown).

Determination of the Zn(II) Content of the Enzymes. The metal content in the samples of DCH and 3H mutants was determined under denaturing conditions using the colorimetric metal chelator 4-(2-pyridylazo)resorcinol (PAR) as described previously (*27*).

Steady State Kinetic Assays. The kinetic parameters for the hydrolysis of different β-lactam antibiotics catalyzed by the DCH and 3H mutants, under steady state conditions, were obtained by determination of the initial rate of reaction at different substrate concentrations. Substrate concentrations were calculated on the basis of the following molar absorptivities: benzylpenicillin, $\Delta\varepsilon_{235} = -775\ M^{-1}\ cm^{-1}$; cefotaxime, $\Delta\varepsilon_{260} = -7500\ M^{-1}\ cm^{-1}$; nitrocefin, $\Delta\varepsilon_{485} = 17420\ M^{-1}\ cm^{-1}$; and imipenem, $\Delta\varepsilon_{300} = -9000\ M^{-1}\ cm^{-1}$. Plots of the dependence of the initial rates on substrate concentration were fit to the Michaelis−Menten equation, using SigmaPlot 8.0. Reactions were carried out in 10 mM HEPES (pH 7.5), 200 mM NaCl, 20 μM $ZnSO_4$, and 0.05 mg/mL BSA at 30 °C. Absorbance changes upon substrate hydrolysis were measured using a Jasco V-550 spectrophotometer, and the temperature was kept constant by means of a PolyScience digital circulator connected to the cell holder in the spectrophotometer.

Solvent Kinetic Isotope Effect Assays. The kinetic parameters obtained for the hydrolysis of different β-lactam antibiotics catalyzed by the DCH and 3H mutants in H_2O, under steady state conditions, were compared with the kinetic parameters obtained for the same reaction carried out in D_2O. The initial rate of hydrolysis at different substrate concentrations was measured in 10 mM HEPES [pD 7.5 (pH 7.1)], 200 mM NaCl, 20 μM $ZnSO_4$, and 0.05 mg/mL BSA at 30 °C. The dependence of the initial rates on substrate concentration was fit to the Michaelis−Menten equation, using SigmaPlot 8.0. The deuterated reaction medium was equilibrated at 30 °C under a N_2 gas atmosphere, prior to reaction. The hydrolysis of antibiotics was registered in open cells, over a period of less than 5 min, to prevent significant uptake of water from the environment.

Preparation of Metal-Free Enzymes. All buffer solutions used to prepare the apoenzymes were treated by being extensively stirred with Chelex 100 (Sigma). Apoprotein samples were prepared by dialysis of the purified holoprotein (approximately 200 μM) against two changes of >100 volumes of 10 mM HEPES (pH 7.5), 200 mM NaCl, and 20 mM EDTA over a 12 h period, with stirring. EDTA was removed from the resulting apoenzyme solution by three dialysis steps, against >100 volumes of 10 mM HEPES (pH 7.5), 1 M NaCl, and Chelex 100, and three dialysis steps against >100 volumes of 10 mM HEPES (pH 7.5), 200 mM NaCl, and Chelex 100 (*19*). All dialyses were carried out at 4 °C. The number of free cysteine thiols in the DCH-BcII apoprotein was determined by reaction with 5,5-dithiobis(2-nitrobenzoic acid) under denaturing conditions (*28*).

Electronic Spectroscopy of Co(II)-BcII Mutants. A solution of 200−300 μM apoprotein in 10 mM HEPES (pH 7.5) and 200 mM NaCl was titrated with a 5−10 mM $CoSO_4$ stock solution prepared in 10 mM HEPES (pH 7.5) and 200 mM NaCl. The spectra were recorded at room temperature in a Jasco V-550 UV−visible spectrophotometer, and difference spectra were obtained by subtracting the spectrum of the corresponding apoprotein. The equivalents of bound Co(II) were calculated as the ratio between the concentration of added Co(II) in the sample and the concentration of protein capable of binding metal, which was calculated by multiplying the concentration of protein determined by absorbance at 280 nm by the factor n, where n is the Zn(II) content of the purified proteins (*19*).

Stopped-Flow Experiments. The variations in the visible spectra of Co(II)-substituted 3H-BcII and Co(II)-substituted DCH-BcII during hydrolysis of benzylpenicillin were followed with an Applied Photophysics SX18-MVR stopped-flow system associated with a photodiode-array detector (Applied Photophysics). The measurements were performed in 100 mM HEPES (pH 7.5) and 200 mM NaCl, at 19 °C. A set of scans was acquired in the wavelength range from 300 to 730 nm, with an integration time of 1.28 ms, during the hydrolysis of 5 and 0.5 mM benzylpenicillin solutions catalyzed by approximately 150 μM protein samples (final concentrations reached in the measurement chamber).

X-ray Absorption Spectroscopy. Samples of BcII for XAS (~1 mM) were prepared with 20% (v/v) glycerol in either 50 mM TAMS (pH 6 or 9) (for 3H-BcII) or 10 mM HEPES (pH 7.5) and 200 mM NaCl (DCH-BcII) and loaded in Lucite cuvettes with 6 μm polypropylene windows, before being rapidly frozen in liquid nitrogen. X-ray absorption spectra were measured at the National Synchrotron Light Source (Brookhaven National Laboratory, Upton, NY), beamline X3B, with a Si(111) double crystal monochromator; harmonic rejection was accomplished using a Ni focusing mirror. Data collection and reduction were accomplished according to published procedures (*29*). The data in Figure 2 represent the average of six to eight scans per sample.

Fourier-filtered EXAFS data were fit utilizing theoretical amplitude and phase functions calculated with FEFF version 8.00 (*30*). The Zn−N and Zn−S scale factors, along with their threshold energies, ΔE_0, were calibrated to the experimental spectrum for tetrakis-1-methylimidazole zinc(II) perchlorate, $Zn(MeIm)_4$, for Zn−N and zinc tetraphenylthiolate, $Zn(SPh)_4$, for Zn−S bonds, and held fixed at their calibrated values ($S_{Zn-N} = 0.78$, $S_{Zn-S} = 0.91$, $\Delta E_0 = -21$ eV for both) in fits to the BcII data presented here. First-shell fits were then obtained for all reasonable coordination

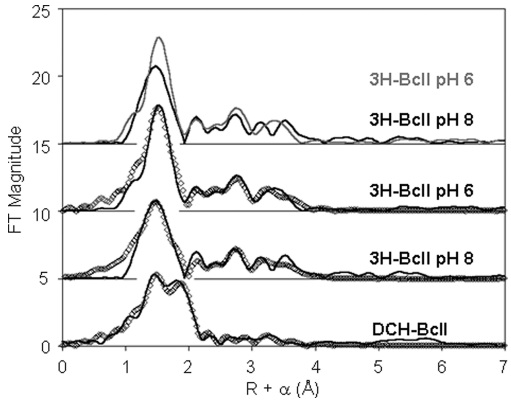

FIGURE 2: Fourier transforms of k^3-weighted EXAFS for 3H-BcII and DCH-BcII. From top to bottom is shown a comparison of 3H-BcII at pH 6 (gray) and pH 8 (black), and best fits for 3H-BcII at pH 6, 3H-BcII at pH 8, and DCH-BcII at pH 7.5. All curves have been offset vertically for clarity. The fitted data are presented as black lines; the fits are presented as open diamonds.

numbers, including mixed N/O/S ligation, while allowing the absorber−scatterer distance, R_{as}, and the Debye−Waller factor, σ_{as}^2, to vary; the best fits are presented in Table 1. Multiple scattering contributions from histidine ligands were fit as described previously (*29*). Metal−metal (Zn−Zn) scattering was modeled with reference to the experimental spectrum of $Zn_2(salpn)_2$.

Paramagnetic NMR Spectroscopy. NMR spectra were recorded on a Bruker Avance II 600 spectrometer operating at 600.13 MHz, at 298 K. ^{1}H NMR spectra were recorded under conditions set to optimize the detection of the fast relaxing paramagnetic resonances, using the superWEFT pulse sequence (*31*). Spectra were acquired over large spectral widths, with acquisition times ranging from 16 to 80 ms and intermediate recovery delays from 2 to 35 ms, and the best combinations of delays were selected. All Co(II)-substituted samples were at least 1 mM in concentration. To obtain spectra in D_2O, samples were diafiltered against the corresponding buffer (prepared in D_2O), containing the same concentration of Co(II) as the protein sample. Amicon-Ultra-4 units (Millipore) were used as diafiltration devices.

RESULTS

Biochemical Characterization of the Mutants 3H-BcII and DCH-BcII. To probe the relevance of the isolated 3H and DCH sites to the Mβ L activity of wild-type BcII, we designed two mutant proteins. In principle, substitution of the metal ligands with Ser residues is expected to significantly impair metal binding, while at the same time preserving a polar environment, without the introduction of a steric perturbation that may interfere with substrate binding. We also wanted to obtain monometallic variants with the smallest number of possible mutations. Since both D120S and C221S single mutants retain the ability to bind more than one Zn(II) ion (*23, 25*), we attempted to completely abolish the DCH site by combining both mutations. This mutant was hence named 3H-BcII. Point mutants at positions 116, 118, and 196 (the 3H site) are also capable of binding more than one Zn(II) ion (*22*). Therefore, with the aim of eliminating the 3H site, DCH-BcII was prepared by substitution of all three ligating histidines with serine residues.

Both BcII mutants were expressed in *E. coli* BL21(DE3)pLysS′ as fusion proteins with GST; the fusion proteins were digested with thrombin, and the BcII variants were then purified to homogeneity from the digestion mixture. The near- and far-UV circular dichroism spectra of purified 3H-BcII and DCH-BcII mutant proteins showed that the protein fold of the WT enzyme was preserved in both cases (data not shown). Thus, major changes in enzyme activity can be attributed to a direct effect of the introduced mutations on catalysis, since the protein scaffold is mostly unaltered in the mutant enzymes.

The total Zn(II) content was determined by a spectrophotometric assay using the colorimetric reagent PAR, after dialysis of the mutant proteins against a metal-free buffer solution. The 3H-BcII mutant binds 1.06 ± 0.03 Zn(II) ions per protein molecule, while the metal content of DCH-BcII ranged from 0.60 to 1.1 Zn(II) ions per molecule (five independent protein preparations). The variations in the metal content of DCH-BcII correlated with the amount of reduced cysteine thiols as determined by reaction with DTNB. These data suggest that replacement of the mentioned metal ligands in the 3H-BcII and DCH-BcII mutant proteins abolished metal binding to the DCH and 3H sites, respectively. Other spectroscopic techniques were employed to verify that we had indeed prepared mononuclear enzymes, with metal bound exclusively at either the 3H or DCH sites.

X-ray Absorption Spectroscopy. EXAFS data were recorded at the zinc edge, and the corresponding Fourier transforms for 3H-BcII and DCH-BcII are shown in Figure 2 (solid lines) along with their best fits (white symbols). EXAFS curve fitting results are presented in Table 1; fits to Fourier-filtered and unfiltered data gave similar results (see Figure S1 and Table 1). The first-shell scattering in 3H-BcII gives rise to a symmetric distribution at both pH 6 and 8, although the main peak is sharper and more intense at pH 6, suggesting either stronger coordination at low pH or a more ordered site at low pH. Similarly, only minimal variation is noted in their XANES spectra, with only a ca. 5% increase in the white line at pH 6 (Figure S2). Fits to Fourier-filtered first-shell scattering do not indicate an increase in overall average bond length, making an increase in coordination number unlikely. In both cases, the data for 3H-BcII indicate coordination to four nitrogen/oxygen donors at an average distance of ~2.00 Å (fit 3). Fits to the low-pH data, using a mixture of one O donor and three N donors, refine to distances of 1.98 and 2.02 Å, respectively. These distances are not sufficiently different to be resolved by the data presented here and suggest that the higher intensity of the main peak in the FT is purely due to a narrower distribution in the low-pH spectrum, possibly due to protonation of the bound water molecule. This is consistent with fits to the high-pH data, which refine separate contributions of one O and three N donors to distances of 1.91 and 2.03 Å, respectively; these distances are within the resolution limits of the data in Figure 2 (ca. 0.10 Å). Both spectra show significant outer shell scattering, and multiple scattering analyses indicate the presence of three histidine ligands in the primary coordination sphere of Zn in 3H-BcII, as expected.

The main peak in the FT for DCH-BcII shows substantial asymmetry, and Fourier-filtered first-shell fits suggest coordination to an average of five nitrogen/oxygen donors at a distance of 2.07 Å. Inclusion of a single sulfur scatterer in the primary coordination sphere results in a dramatic 80% reduction in the fit residual with the asymmetry due to the

Table 1: EXAFS Curve Fitting Results for 3H and DCH Mutants[a]

	model	Zn−O	Zn−N	Zn−S	Zn−His[b]	R_f[c]	R_u
Zn(II) 3H-BcII at pH 6[d]	4N/O		2.01 (2.3)			11	228
	1O + 3N	1.98 (13)	2.02 (0.6)			6	188
	1N/O + 3His		2.01 (2.6)		2.91 (2.9), 3.13 (10)		
					4.08 (12), 4.38 (19)	46	88
Zn(II) 3H-BcII at pH 8[e]	4N/O		2.00 (2.6)			26	332
	1O + 3N	1.91 (2.0)	2.03 (3.0)			14	275
	1N/O + 3His	1.91 (2.5)	2.03 (3.4)		2.91 (4.4), 3.13 (4.3)		
					4.14 (17), 4.37 (15)	84	136
Zn(II) DCH-BcII[f]	5N/O		2.07 (10)			102	430
	4N/O + 1S		2.02 (6.0)	2.28 (2.7)		22	81
	3 N/O + 1His + 1S		2.02 (5.9)	2.28 (2.6)	2.89 (9.7), 3.18 (3.8)		
					4.06 (13), 4.45 (15)	24	56

[a] Distances (angstroms) and disorder parameters [in parentheses, σ^2 ($\times 10^{-3}$ Å^2)] derive from integer coordination number fits to Fourier-filtered EXAFS data. [b] Multiple scattering paths represent combined scattering paths described in Experimental Procedures. [c] Goodness of fit (R_f for fits to filtered data, R_u for fits to unfiltered data) defined as $1000\sum_{i=1}^{N}\{[\mathrm{Re}(\chi_{i_{calc}})]^2 + [\mathrm{Im}(\chi_{i_{calc}})]^2\}/\sum_{i=1}^{N}\{[\mathrm{Re}(\chi_{i_{obs}})]^2 + [\mathrm{Im}(\chi_{i_{obs}})]^2\}$, where N is the number of data points. [d] For 3H-BcII at pH 6, k = [1.2, 13.5]; R = [0.8, 2.0] for first-shell fits; and R = [0.1, 4.4] for ms fits. [e] For 3H-BcII at pH 8, k = [1.2, 13.1]; R = [0.8, 2.0] for first-shell fits; and R = [0.1, 4.4] for ms fits. [f] For DCH-BcII, k = [1.2, 13.5]; R = [0.8, 2.2] for first-shell fits; and R = [0.1, 4.4] for ms fits.

presence of a mixed N/O/S coordination sphere, consistent with the lone Zn(II) ion coordinated at the DCH site. The outer shell scattering for DCH-BcII is significantly lower in amplitude than that of 3H-BcII, and multiple scattering analysis indicates ligation to one histidine residue. These data show no indication of a missing component in the fit, such as that expected from carbon of a bidentate carboxylate; however, such an interaction is likely to be overwhelmed by the Zn−S scattering. Thus, these data cannot rule out bidentate coordination of the aspartate. Inclusion of a Zn−Zn interaction failed to improve the fits, for either 3H-BcII or DCH-BcII, allowing us to rule out the existence of a dimetallic site in both mutants.

Spectroscopic Characterization of the Co(II) Derivatives. To better characterize the coordination sphere of the two mutant proteins, we obtained the corresponding Co(II) derivatives. The UV−vis spectra of these derivatives, obtained upon addition of excess Co(II) to the corresponding mutant apoenzymes, are compared to the spectrum of di-Co(II) WT BcII (*11, 19*) (Figure 3). The molar absorptivity and number of Co(II) equivalents were calculated considering the concentration of protein capable of binding metal, as described in Experimental Procedures.

The spectrum of Co(II) 3H-BcII presented a pattern of overlapping bands in the 450−650 nm region of the spectrum, which can be assigned to ligand field bands (Figure 3A). These d−d bands presented a maximum at 546 nm, with an estimated extinction coefficient of 138 M^{-1} cm^{-1} (Figure 3B), which is indicative of a pentacoordinate Co(II) site in 3H-BcII. The absence of the intense feature in the UV range observed in WT BcII (300−400 nm) is consistent with the removal of Cys221 as a metal ligand (Figure 3A). This residue is responsible for a ligand-to-metal charge transfer transition in Co-substituted WT BcII. The intensity of the ligand field bands increased with a hyperbolic shape (Figure 3B). After addition of 1.5 equiv of Co(II), there was no further increase in the intensity of the d−d bands.

The ^{1}H NMR spectra of Co(II)-substituted 3H-BcII, recorded under conditions that allow the detection of paramagnetic signals, revealed a set of three isotropically shifted resonances from 40 to 80 ppm (Figure 4), which are consistent with a metal site of low magnetic anisotropy, i.e., tetra- or pentacoordinate. One of the three signals (signal a)

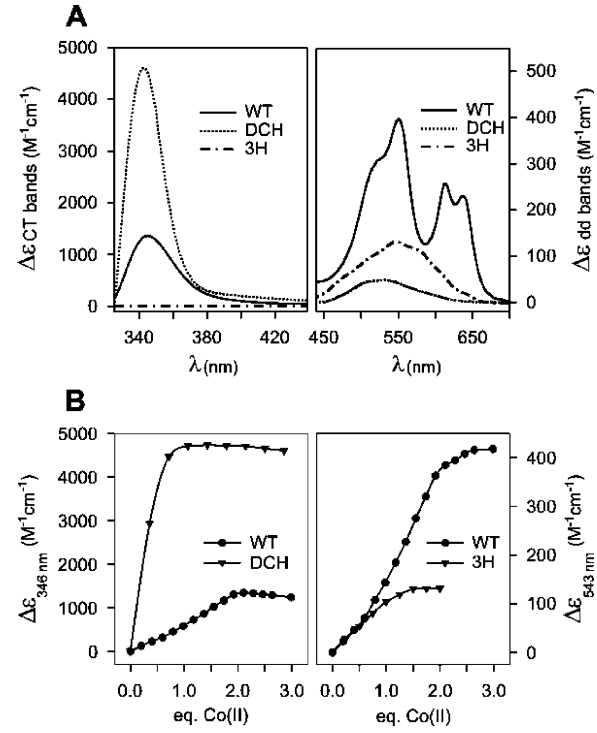

FIGURE 3: Electronic spectroscopy of the Co(II) derivatives of DCH and 3H-BcII. (A) UV−vis spectra of mono-Co(II) DCH and mono-Co(II) 3H [upon addition of 1 equiv of Co(II) to the mutant apoenzymes] compared with that previously reported for di-Co(II) BcII (*19*). (B) Plot of the molar absorption at 346 (left) and 543 nm (right) as a function of Co(II) equivalents added to the apoproteins in the UV−vis titration. Molar absorption and the number of Co(II) equivalents were calculated considering the concentration of protein capable of binding metal, as described in Experimental Procedures. The titrations were performed in 10 mM HEPES and 200 mM NaCl (pH 7.5), with protein concentrations of 210 μM apo-DCH and 230 μM apo-3H.

is absent in the spectrum of the protein sample dissolved in D_2O, indicating that at least one histidine residue is coordinated to the Co(II) ion. The ^{1}H NMR data allow identification of only one exchangeable imidazolic proton, while two were found in the wild-type protein (of three His ligands in this site). These differences can be attributed to a greater extent of solvent exposure of the metal site in the absence of one metal ion, which might induce a larger NH exchange rate with the bulk solvent. No signals were detected at

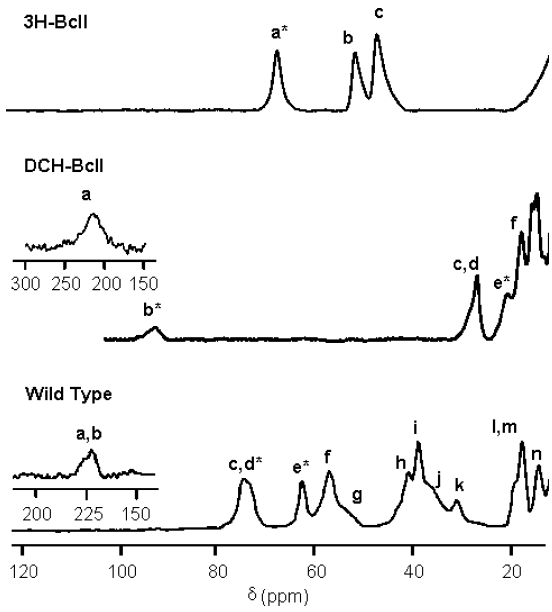

FIGURE 4: ^{1}H NMR spectra of Co(II)-substituted wild-type BcII (bottom), DCH-BcII (middle), and 3H-BcII (top). All spectra were recorded at 298 K with a superWEFT pulse sequence. 3H and DCH were in TAMS buffer (pH 6), while WT BcII was in 100 mM HEPES buffer and 200 mM NaCl. The total recycle time and the recovery delay of the superWEFT experiments were 70 and 10 ms, respectively, for experiments in the 120−10 ppm spectral window, and 25 and 5 ms, respectively, for experiments in the 300−120 ppm window. Signals marked with an asterisk were not observed when the samples were dissolved in buffer prepared with 100% D_2O.

chemical shifts larger than 120 ppm, consistent with the absence of the Cys221 residue as a metal ligand. The remaining resonances are expected to arise from nonexchangeable imidazolate protons.

The electronic spectrum of Co(II) DCH-BcII also exhibited a pattern of overlapping bands in the 450−650 nm region of the spectrum, and these are similarly assigned to Co(II) ligand field bands (Figure 3A). The d−d bands presented a maximum at 520 nm, with an extinction coefficient of ca. 40 M^{-1} cm^{-1}, which suggests a hexacoordinate Co(II) site in DCH-BcII. An intense absorption band centered at 346 nm can be attributed to a Cys221−Co(II) charge transfer band (Figure 3A). The extinction coefficient estimated for this transition in DCH-BcII correlates well with the values reported in the literature for S → Co(II) charge transfer bands and is at least 4 times more intense than that observed for WT BcII. The intensity of the LMCT band increased almost linearly until a 1:1 Co(II):enzyme ratio was obtained (Figure 3B). After the addition of 1 equiv of Co(II), there was no further increase in the intensity of either the LMCT or the d−d bands.

The ^{1}H NMR spectrum of Co(II)-substituted DCH-BcII revealed a downfield nonexchangeable signal characteristic of the β-CH_2 protons of a Co(II)-bound cysteinate (signal A). Signals D and F were assigned to the two geminal Cβ protons of Asp120, since a strong cross-peak in a NOESY spectrum was observed (not shown). Signal B was assigned to an imidazole NH group from His263 on the basis of its absence in D_2O and its chemical shift. The signal spreading observed in the NMR spectrum (from 100 to 20 ppm) is consistent with a pentacoordinate Co(II) ion in DCH-BcII (*32*).

Enzymatic Characterization of 3H-BcII and DCH-BcII Mutants. The hydrolytic capabilities of the two mutants were tested against different β-lactam substrates under steady state conditions. Lactamase activity was severely impaired in both mutants, against all substrates assayed (Table 2). 3H-BcII exhibited k_{cat}/K_M values 4−5 orders of magnitude lower than those reported for WT BcII. The DCH-BcII mutant revealed a decrease of 3−4 orders of magnitude in catalytic efficiency compared to that of WT BcII. In most cases, both mutants displayed a decrease in k_{cat} and an increase in K_M, with the decrease in catalytic efficiency mainly governed by the large variations in k_{cat} (Figure 5).

The solvent kinetic isotope effect (SKIE, $^Dk_{cat}$) was studied for the mutant proteins and compared with those observed for WT BcII, by determining the steady state catalytic parameters in H_2O and D_2O for nitrocefin, cefotaxime, and benzylpenicillin (Table 2). Both 3H-BcII and DCH-BcII exhibited normal SKIEs ($^Dk_{cat} > 1$) with the substrates assayed, as previously observed in WT BcII, indicating that in these two mutants the rate-limiting step also involves a proton transfer. In particular, the SKIE measured for DCH-BcII is very similar to that observed in the dinuclear wild-type enzyme.

The hydrolysis of benzylpenicillin by the Co(II)-substituted forms of 3H-BcII and DCH-BcII was followed by time-resolved UV−vis spectra acquired with a photodiode array coupled to a stopped-flow mixing device, with substrate:enzyme ratios of 30:1 and 3:1. No changes were observed in the electronic spectra of the proteins in either case, in the time frame required for complete substrate hydrolysis (Figure 6). These results contrast with those observed in the Co(II)-substituted wild-type enzyme, where the electronic spectra of the protein suffered major changes during the reaction. Such changes were assigned to the accumulation of different intermediates during the reaction, which suggests that changes in the cordination geometry of the metal center took place during turnover (*33, 34*).

DISCUSSION

The assessment of the relative activities of mono- and dinuclear sites in MβL-mediated catalysis has been one of the most controversial issues in the studies of the class B1 enzymes, particularly BcII (*11, 20, 22*). We recall that BcII was originally crystallized with a single metal ion bound, at the 3H site (Figure 1A) (*10*). Subsequent spectroscopic studies revealed that BcII could also bind a second metal ion as observed with B1 enzymes (*11*), which was later confirmed by a structure determined from crystals grown in the presence of excess Zn(II) (Figure 1B) (*12*). The latter showed two metal binding sites identical to that observed in the structures of other B1 MβLs, such as CcrA and IMP-1 (*35, 36*). These results have led to a discussion regarding the catalytically and biologically relevant form of this enzyme. This confusion arises, in large part, from the fact that the apoenzyme, the mononuclear species, and the dinuclear species coexist over a wide range of metal:enzyme ratios (*19–21*). In addition, the mononuclear enzyme in solution is a mixture of two states in equilibrium in which the metal ion is located in the 3H and DCH site. Thus, a single mononuclear BcII species cannot be isolated and hence cannot be subjected to kinetic studies on its own.

Table 2: Kinetic Parameters for Hydrolysis of Nitrocefin, Cefotaxime, Benzylpenicillin, and Imipenem by WT BcII, 3H-BcII, and DCH-BcII[a]

	k_{cat} (s^{-1})	K_M (mM)	k_{cat}/K_M (s^{-1} M^{-1})	$^{H_2O}k_{cat}/^{D_2O}k_{cat}$
		Nitrocefin		
WT	7.9 ± 0.7	5.7 ± 0.3	$(1.4 \pm 0.1) \times 10^6$	1.4 ± 0.1
3H	0.46 ± 0.04	630 ± 40	$(7.0 \pm 0.9) \times 10^2$	4 ± 1
DCH	0.21 ± 0.02	220 ± 40	$(9 \pm 2) \times 10^2$	ND
		Benzylpenicillin		
WT	262 ± 27	510 ± 30	$(5.1 \pm 0.2) \times 10^5$	1.4 ± 0.1
3H	0.054 ± 0.001	440 ± 60	$(1.2 \pm 0.2) \times 10^2$	ND
DCH	0.94 ± 0.03	5700 ± 400	$(1.7 \pm 0.2) \times 10^2$	1.0 ± 0.1
		Cefotaxime		
WT	67 ± 1	42 ± 3	$(1.6 \pm 0.1) \times 10^6$	1.6 ± 0.1
3H	0.029 ± 0.002	460 ± 60	$(6.0 \pm 1.0) \times 10$	4 ± 1
DCH	0.10 ± 0.01	130 ± 20	$(7.2 \pm 1.2) \times 10^2$	1.5 ± 0.1
		Imipenem		
WT	110 ± 10	660 ± 70	$(1.7 \pm 0.2) \times 10^5$	ND
3H	1.0 ± 0.1	$(7 \pm 1) \times 10^3$	$(1.4 \pm 0.4) \times 10^2$	ND
DCH	1.3 ± 0.2	2100 ± 500	$(6 \pm 2) \times 10^2$	ND

[a] Parameters were determined by fitting initial reaction rates against substrate concentration. The experiments were carried out in 10 mM HEPES (pH 7.5), 200 mM NaCl, 50 μg/mL BSA, and 20 μM Zn(II) in the case of WT BcII and DCH-BcII. In the case of 3H-BcII, the experiments were carried out in 10 mM HEPES (pH 7.5), 200 mM NaCl, and 50 μg/mL BSA. For 3H-BcII, the same k_{cat}/K_M values were obtained with increasing Zn(II) concentrations (from 20 to 100 μM).

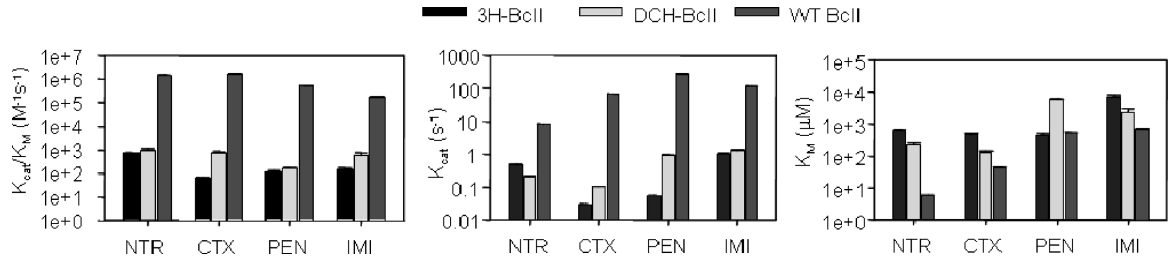

FIGURE 5: Charts comparing k_{cat}/K_M, k_{cat}, and K_M for hydrolysis of nitrocefin (NTR), cefotaxime (CTX), benzylpenicillin (PEN), and imipenem (IMI) by 3H-BcII (black bars), DCH-BcII (light gray bars), and WT BcII (dark gray bars).

We have designed two BcII mutants in an attempt to create localized mononuclear variants. Several mutagenesis studies indicate that substitution of single metal ligands of either metal site, one at a time, does not render mononuclear forms of BcII (*22, 23*). Hence, we decided to mutate at least two metal ligands from each site. The mutant protein 3H-BcII was obtained by substitution of two metal ligands from the DCH site, residues Asp120 and Cys221, with Ser residues. Serine residues are rarely found as first-shell metal ligands in Zn(II) enzymes but are fully capable of preserving hydrogen bond networks (*37*). We then expected that the DCH binding site would be abolished in 3H-BcII. To eliminate the 3H site, we mutated residues His116, His118, and His196 to serine residues. This variant was named DCH-BcII.

3H-BcII and DCH-BcII presented only one metal ion bound per enzyme molecule, as determined by the spectrophotometric assay with the colorimetric metal chelator PAR. The spectroscopic studies of the Zn(II) and Co(II) derivatives of 3H-BcII confirmed that in this protein variant a single metal ion was bound to three histidine residues, most likely His116, His118, and His196. In WT BcII, the metal is tetrahedrally coordinated by three His residues and a water molecule (*12*). In contrast to the ligand binding environment observed with WT BcII, the EXAFS data on Zn(II) 3H-BcII and the absorption coefficients of the ligand field bands in the Co(II) derivative indicate that the metal ion presents a pentacoordinate geometry. It is very likely that in this mutant, the coordination sphere of the metal ion has been expanded by inclusion of an additional solvent molecule. This situation resembles that found for carbonic anhydrase, which presents a similar 3H site, at low pH. In HCA I, the metal site is pentacoordinate with three histidines and two H_2O/OH^- molecules at low pH and becomes tetracoordinate at high pH due to the loss of one water (*38*). If this were the case for 3H-BcII, at high pH the zinc site in this mutant should be equivalent to the wild-type 3H site. However, we do not observe changes in the NMR and visible spectra of the Co(II)-containing mutant at pH 9, indicating there is no change in coordination geometry. Accordingly, there was no significant increase in catalytic efficiency.

Spectroscopic studies of the Zn(II) and Co(II) derivatives of DCH-BcII are indicative of a single, pentacoordinate metal ion bound to Asp120, Cys221, and His263. As in the case of WT BcII, we propose that the coordination sphere is completed by two solvent molecules. The optical spectrum of Co(II)-substituted DCH-BcII reveals two main differences with the native DCH site present in WT BcII (*11*). The ligand field bands are more intense than those observed for Co(II) bound in the DCH site in the $Zn_{3H}-Co_{DCH}$ WT BcII adduct obtained at pH 6 (*11*), which suggests a metal site with a lower coordination number or greater distortion at the DCH site. More interestingly, the intensity of the Cys221 $\rightarrow$ Co(II) charge transfer band is 4 times larger than the intensity of the band observed in WT BcII (pH 6 and 7.5) (*11, 19*). In fact, the extinction coefficient of the LMCT band in DCH-BcII is in better agreement with the values commonly observed for this kind of electronic transition in other

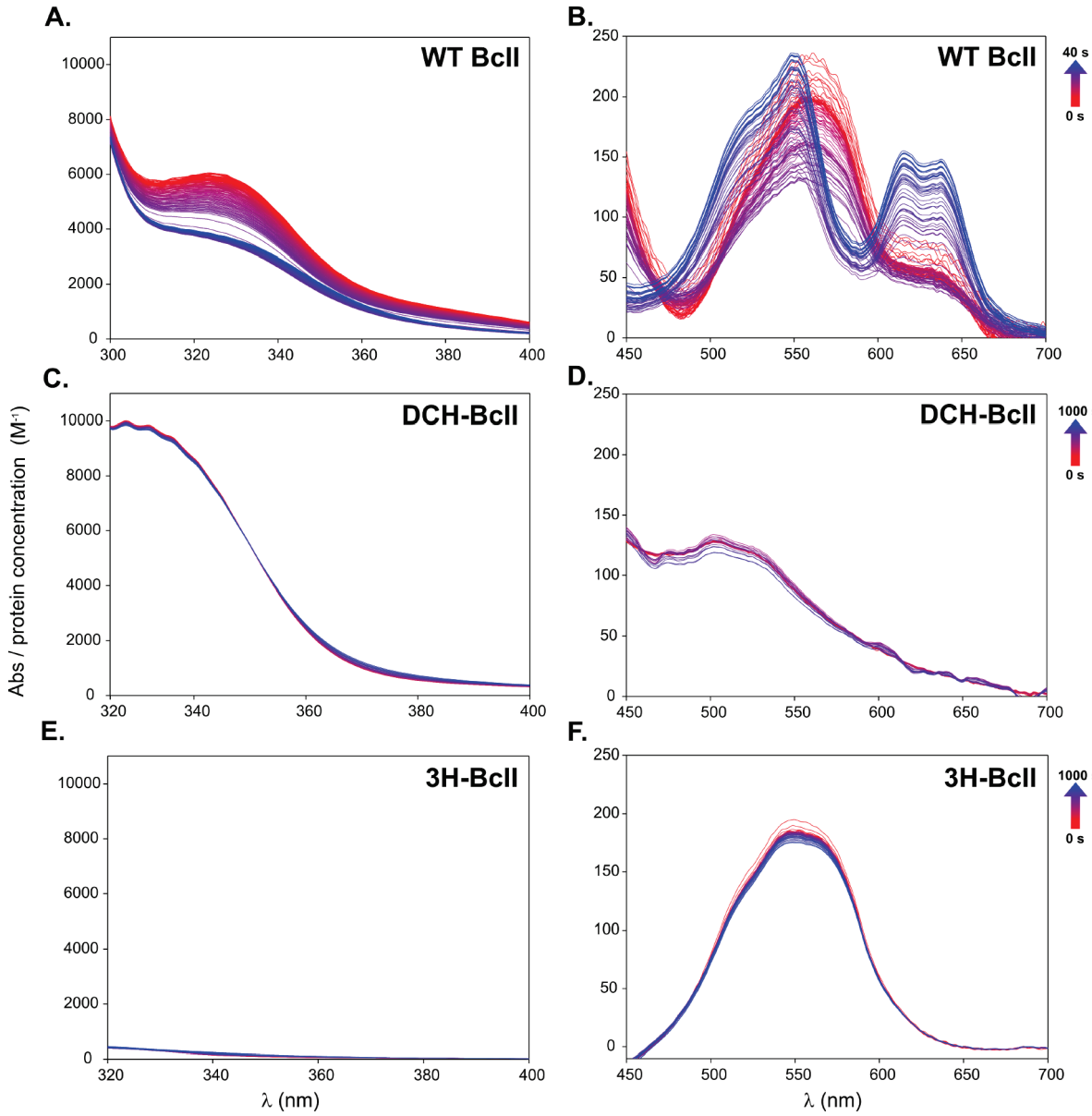

FIGURE 6: Rapid-scanning stopped-flow spectra of Co(II)-substituted wild-type BcII (A and B), DCH-BcII (C and D), and 3H-BcII (E and F) during the hydrolysis of penicillin G. Panels A, C, and E show the UV regions of the electronic spectra (where the charge transfer band is observed), while panels B, D, and F show the visible regions (where the ligand field bands are observed). Absorbance values are normalized by the concentration of protein used in each experiment. Experiments were carried out at 6 °C for the wild-type protein and at 19 °C for both mutants.

metalloenzymes and in model complexes (*39*). The spectrum closely resembles that of Co(II)-substituted farnesyltransferase, in which the metal ion adopts a five-coordinate geometry with an Asp, Cys, and His protein ligand set (*40*), confirming the structure of the engineered site.

The kinetic studies of 3H- and DCH-BcII showed that neither mononuclear mutant was a viable lactamase. The fast kinetic studies followed by UV−vis spectroscopy reveal that this residual activity is not accompanied by changes in the metal sites in either mutant. Therefore, this activity cannot be correlated with the one observed in the wild-type enzyme or in partially active mutants. Residual activity has been detected in cases where all active site residues were removed (*41*) and can be attributed to a medium effect (*42*). These results suggest that removal of either metal binding site and/or the involved residues results in virtually inactive β-lactamases.

The 3H site has been suggested to provide the attacking nucleophile, while the DCH site has been implicated in substrate binding (*43*) and C−N bond cleavage (*44, 45*). The lower K_M values estimated for DCH-BcII (with the exception of benzylpenicillin), compared with those of 3H-BcII, are in accordance with the proposed role of the DCH site in substrate binding. However, the very low catalytic efficiency displayed by DCH-BcII compared to that of the wild-type enzyme reveals the importance of the residues of the 3H site for the activity of the mononuclear enzymes in which the metal ion is localized in the DCH site.

CphA, a subclass B2 MβL, presents a single metal ion bound to the DCH site and is active only in this mononuclear form. On the basis of the structure of the complex of CphA with hydrolyzed biapenem, a catalytic mechanism was proposed for CphA (*17*). According to this mechanism, the nucleophile would be a water molecule activated through

hydrogen bond interactions with His118, one of the ligands of the 3H site in BcII. A similar situation has been proposed for the recently characterized enzyme GOB from *Elizabethkingia meningosepticum*, which also behaves as a mononuclear lactamase lacking a metal ion at the 3H site (*15*). Hence, the disruption of the hydrogen bond network on DCH-BcII could explain the low activity exhibited by this variant.

The very low activity of the two mononuclear variants studied here can be attributed assuming two possible scenarios: (1) that only the dinuclear species is active, as recently suggested by Badarau and Page (*46*), or (2) that the mononuclear variants can be active only if aided by other residues that would be metal ligands in the dinuclear species. For instance, occupation of the 3H site would yield an active species, providing a metal-activated nucleophile, only if Asp120 and Cys221 participate in the hydrogen bond network of this nucleophile (*47*). On the other hand, the DCH site would be active only if other residues (such as His118 and His196) participated in the activation of a non-metal-bound nucleophilic moiety. Thus, the two metal binding sites could be modularly exploited to render different active forms. Experiments are underway to test this hypothesis.

SUPPORTING INFORMATION AVAILABLE

Figure S1 showing unprocessed k^3-weighted EXAFS for 3H- and DCH-BcII and Figure S2 showing normalized Zn XANES spectra for 3H- and DCH-BcII. This material is available free of charge via the Internet at http://pubs.acs.org.

REFERENCES

1. Fisher, J. F., Meroueh, S. O., and Mobashery, S. (2005) Bacterial resistance to β-lactam antibiotics: Compelling opportunism, compelling opportunity. *Chem. Rev. 105*, 395–424.
2. Wilke, M. S., Lovering, A. L., and Strynadka, N. C. (2005) β-Lactam antibiotic resistance: A current structural perspective. *Curr. Opin. Microbiol. 8*, 525–533.
3. Helfand, M. S., and Bonomo, R. A. (2003) β-Lactamases: A survey of protein diversity. *Curr. Drug Targets: Infect. Disord. 3*, 9–23.
4. Crowder, M. W., Spencer, J., and Vila, A. J. (2006) Metallo-β-lactamases: Novel Weaponry for Antibiotic Resistance in Bacteria. *Acc. Chem. Res. 39*, 721–728.
5. Wang, Z., Fast, W., Valentine, A. M., and Benkovic, S. J. (1999) Metallo-β-lactamase: Structure and mechanism. *Curr. Opin. Chem. Biol. 3*, 614–622.
6. Sulton, D., Pagan-Roderiguez, D., Zhou, X., Liu, Y., Hujer, A. M., Bethel, C. R., Helfand, M. S., Thomson, J. M., Anderson, V. E., Buynak, J. D., Ng, L. M., and Bonomo, R. A. (2005) Clavulanic acid inactivation of SHV-1 and the inhibitor resistant SER130GLY SHV-1β-lactamase: Insights into the mechanism of inhibition. *J. Biol. Chem. 280*, 35528–35536.
7. Toney, J. H., and Moloughney, J. G. (2004) Metallo-β-lactamase inhibitors: Promise for the future? *Curr. Opin. Invest. Drugs 5*, 823–826.
8. Galleni, M., Lamotte-Brasseur, J., Rossolini, G. M., Spencer, J., Dideberg, O., and Frere, J. M. (2001) Standard numbering scheme for class B β-lactamases. *Antimicrob. Agents Chemother. 45*, 660–663.
9. Garau, G., Garcia-Saez, I., Bebrone, C., Anne, C., Mercuri, P., Galleni, M., Frere, J. M., and Dideberg, O. (2004) Update of the standard numbering scheme for class B β-lactamases. *Antimicrob. Agents Chemother. 48*, 2347–2349.
10. Carfi, A., Pares, S., Duee, E., Galleni, M., Duez, C., Frère, J. M., and Dideberg, O. (1995) The 3-D structure of a zinc metallo-β-lactamase from *Bacillus cereus* reveals a new type of protein fold. *EMBO J. 14*, 4914–4921.
11. Orellano, E. G., Girardini, J. E., Cricco, J. A., Ceccarelli, E. A., and Vila, A. J. (1998) Spectroscopic characterization of a binuclear metal site in *Bacillus cereus* β-lactamase II. *Biochemistry 37*, 10173–10180.
12. Fabiane, S. M., Sohi, M. K., Wan, T., Payne, D. J., Bateson, J. H., Mitchell, T., and Sutton, B. J. (1998) Crystal structure of the zinc-dependent β lactamase from *Bacillus cereus* at 1.9 Å resolution: Binuclear active site with features of a mononuclear enzime. *Biochemistry 37*, 12404–12411.
13. Garcia-Saez, I., Mercuri, P. S., Papamicael, C., Kahn, R., Frere, J. M., Galleni, M., Rossolini, G. M., and Dideberg, O. (2003) Three-dimensional structure of FEZ-1, a monomeric subclass B3 metallo-β-lactamase from *Fluoribacter gormanii*, in native form and in complex with D-captopril. *J. Mol. Biol. 325*, 651–660.
14. Ullah, J. H., Walsh, T. R., Taylor, I. A., Emery, D. C., Verma, C. S., Gamblin, S. J., and Spencer, J. (1998) The crystal strucuture of the L1 metallo-β-lactamase from *Stenotrophomonas maltophilia* at 1.7 Å resolution. *J. Mol. Biol. 284*, 125–136.
15. Moran-Barrio, J., Gonzalez, J. M., Lisa, M. N., Costello, A. L., Peraro, M. D., Carloni, P., Bennett, B., Tierney, D. L., Limansky, A. S., Viale, A. M., and Vila, A. J. (2007) The Metallo-β-lactamase GOB Is a Mono-Zn(II) Enzyme with a Novel Active Site. *J. Biol. Chem. 282*, 18286–18293.
16. Hernández Valladares, M., Felici, A., Weber, G., Adolph, H. W., Zeppezauer, M., Rossolini, G. M., Amicosante, G., Frère, J. M., and Galleni, M. (1997) Zn(II) dependence of the *Aeromonas hydrophila* AE036 metallo-β-lactamase activity and stability. *Biochemistry 36*, 11534–11541.
17. Garau, G., Bebrone, C., Anne, C., Galleni, M., Frere, J. M., and Dideberg, O. (2005) A metallo-β-lactamase enzyme in action: Crystal structures of the monozinc carbapenemase CphA and its complex with biapenem. *J. Mol. Biol. 345*, 785–795.
18. Crawford, P. A., Yang, K. W., Sharma, N., Bennett, B., and Crowder, M. W. (2005) Spectroscopic studies on cobalt(II)-substituted metallo-β-lactamase ImiS from *Aeromonas veronii* bv. *sobria*. *Biochemistry 44*, 5168–5176.
19. Llarrull, L. I., Tioni, M. F., Kowalski, J., Bennett, B., and Vila, A. J. (2007) Evidence for a dinuclear active site in the metallo-β-lactamase BcII with substoichiometric Co(II). A new model for metal uptake. *J. Biol. Chem. 282*, 30586–30595.
20. de Seny, D., Heinz, U., Wommer, S., Kiefer, M., Meyer-Klaucke, W., Galleni, M., Frere, J. M., Bauer, R., and Adolph, H. W. (2001) Metal ion binding and coordination geometry for wild type and mutants of metallo-β-lactamase from *Bacillus cereus* 569/H/9 (BcII): A combined thermodynamic, kinetic, and spectroscopic approach. *J. Biol. Chem. 276*, 45065–45078.
21. Hemmingsen, L., Damblon, C., Antony, J., Jensen, M., Adolph, H. W., Wommer, S., Roberts, G. C., and Bauer, R. (2001) Dynamics of mononuclear cadmium β-lactamase revealed by the combination of NMR and PAC spectroscopy. *J. Am. Chem. Soc. 123*, 10329–10335.
22. Seny, D., Prosperi-Meys, C., Bebrone, C., Rossolini, G. M., Page, M. I., Noel, P., Frere, J. M., and Galleni, M. (2002) Mutational analysis of the two zinc-binding sites of the *Bacillus cereus* 569/H/9 metallo-β-lactamase. *Biochem. J. 363*, 687–696.
23. Paul-Soto, R., Bauer, R., Frere, J. M., Galleni, M., Meyer-Klaucke, W., Nolting, H., Rossolini, G. M., de Seny, D., Hernandez-Valladares, M., Zeppezauer, M., and Adolph, H. W. (1999) Mono- and binuclear Zn^{2+}-β-lactamase. Role of the conserved cysteine in the catalytic mechanism. *J. Biol. Chem. 274*, 13242–13249.
24. Sambrook, J., Fitsch, E. F., and Maniatis, T. (1989) *Molecular Cloning. A Laboratory Manual*, Cold Spring Harbor Laboratory Press, Plainview, NY.
25. Llarrull, L. I., Fabiane, S. M., Kowalski, J. M., Bennett, B., Sutton, B. J., and Vila, A. J. (2007) Asp-120 Locates Zn2 for Optimal Metallo-β-lactamase Activity. *J. Biol. Chem. 282*, 18276–18285.
26. Cricco, J. A. (2002) Role of a Cys Residue in the Structure and Function of Metallo-β-Lactamases. Ph.D. Thesis, University of Rosario, Rosario, Argentina.
27. Hunt, J. B., Neece, S. H., and Ginsburg, A. (1985) The use of 4-(2-pyridylazo)resorcinol in studies of zinc release from *Escherichia coli* aspartate transcarbamoylase. *Anal. Biochem. 146*, 150–157.
28. Ellman, G. L. (1959) Tissue sulfhydryl groups. *Arch. Biochem. Biophys. 82*, 70–77.
29. Costello, A., Periyannan, G., Yang, K. W., Crowder, M. W., and Tierney, D. L. (2006) Site-selective binding of Zn(II) to metallo-β-lactamase L1 from *Stenotrophomonas maltophilia*. *J. Biol. Inorg. Chem. 11*, 351–358.

30. Ankudinov, A. L., Ravel, B., Rehr, J. J., and Conradson, S. D. (1998) Real-space multiple-scattering calculation and interpretation of X-ray-absorption near-edge structure. *Phys. Rev. B 58*, 7565–7576.
31. Inubushi, T., and Becker, E. D. (1983) Efficient detection of paramagnetically shifted NMR resonances by optimizing the WEFT pulse sequence. *J. Magn. Reson. 51*, 128–133.
32. Bertini, I., Turano, P., and Vila, A. J. (1993) NMR of paramagnetic metalloproteins. *Chem. Rev. 93*, 2833–2932.
33. Bicknell, R., and Waley, S. G. (1985) Cryoenzymology of *Bacillus cereus* β-lactamase II. *Biochemistry 24*, 6876–6887.
34. Llarrull, L. I., Tioni, M. F., and Vila, A. J. (2008) Metal Content and Localization during Turnover in *B. cereus* Metallo-β-Lactamase (submitted for publication).
35. Concha, N., Rasmussen, B. A., Bush, K., and Herzberg, O. (1996) Crystal structure of the wide-spectrum binuclear zinc β-lactamase from *Bacteroides fragilis*. *Structure 4*, 823–836.
36. Concha, N. O., Janson, C. A., Rowling, P., Pearson, S., Cheever, C. A., Clarke, B. P., Lewis, C., Galleni, M., Frere, J. M., Payne, D. J., Bateson, J. H., and Abdel-Meguid, S. S. (2000) Crystal structure of the IMP-1 metallo β-lactamase from *Pseudomonas aeruginosa* and its complex with a mercaptocarboxylate inhibitor: Binding determinants of a potent, broad-spectrum inhibitor. *Biochemistry 39*, 4288–4298.
37. Alberts, I. L., Nadassy, K., and Wodak, S. J. (1998) Analysis of zinc binding sites in protein crystal structures. *Protein Sci. 7*, 1700–1716.
38. Bertini, I., Lanini, G., and Luchinat, C. (1983) Equilibrium species in cobalt(II) carbonic anhydrase. *J. Am. Chem. Soc. 105*, 5116–5118.
39. Lever, A. B. P. (1984) *Inorganic Electronic Spectroscopy*, Elsevier, Amsterdam.
40. Huang, C. C., Casey, P. J., and Fierke, C. A. (1997) Evidence for a catalytic role of zinc in protein farnesyltransferase. Spectroscopy of Co^{2+}-farnesyltransferase indicates metal coordination of the substrate thiolate. *J. Biol. Chem. 272*, 20–23.
41. Carter, P., and Wells, J. A. (1990) Functional interaction among catalytic residues in subtilisin BPN′. *Proteins 7*, 335–342.
42. Cannon, W. R., and Benkovic, S. J. (1998) Solvation, reorganization energy, and biological catalysis. *J. Biol. Chem. 273*, 26257–26260.
43. Gonzalez, J. M., Medrano Martin, F. J., Costello, A. L., Tierney, D. L., and Vila, A. J. (2007) The Zn2 Position in Metallo-β-Lactamases is Critical for Activity: A Study on Chimeric Metal Sites on a Conserved Protein Scaffold. *J. Mol. Biol. 373*, 1141–1156.
44. Wang, Z., Fast, W., and Benkovic, S. J. (1999) On the mechanism of the metallo-β-lactamase from *Bacteroides fragilis*. *Biochemistry 38*, 10013–10023.
45. Spencer, J., Read, J., Sessions, R. B., Howell, S., Blackburn, G. M., and Gamblin, S. J. (2005) Antibiotic recognition by binuclear metallo-β-lactamases revealed by X-ray crystallography. *J. Am. Chem. Soc. 127*, 14439–14444.
46. Badarau, A., and Page, M. I. (2006) Enzyme Deactivation Due to Metal-Ion Dissociation during Turnover of the Cobalt-β-Lactamase Catalyzed Hydrolysis of β-Lactams. *Biochemistry 45*, 11012–11020.
47. Dal Peraro, M., Vila, A. J., and Carloni, P. (2002) Structural determinants and hydrogen-bond network of the mononuclear zinc(II)-β-lactamase active site. *J. Biol. Inorg. Chem. 7*, 704–712.
48. Dal Peraro, M., Llarrull, L. I., Rothlisberger, U., Vila, A. J., and Carloni, P. (2004) Water-assisted reaction mechanism of monozinc β-lactamases. *J. Am. Chem. Soc. 126*, 12661–12668.
49. Simona, F., Magistrato, A., Vera, D. M., Garau, G., Vila, A. J., and Carloni, P. (2007) Protonation state and substrate binding to B2 metallo-β-lactamase CphA from *Aeromonas hydrofila*. *Proteins 69*, 595–605.

BI8006912